NANO LETTERS
Letter
Cite This: Nano Lett. 2019, 19, 441−448
pubs.acs.org/NanoLett

Engineered Paramagnetic Graphene Quantum Dots with Enhanced Relaxivity for Tumor Imaging

Yuqi Yang,[†] Shizhen Chen,[†] Haidong Li,[†] Yaping Yuan,[†] Zhiying Zhang,[†] Junshuai Xie,[†] Dennis W. Hwang,[§] Aidong Zhang,[∥] Maili Liu,[†] and Xin Zhou*[,†]

[†]State Key Laboratory of Magnetic Resonance and Atomic and Molecular Physics, National Center for Magnetic Resonance in Wuhan, Wuhan Institute of Physics and Mathematics, Chinese Academy of Sciences, Wuhan, 430071, P.R. China

[§]Department of Chemistry and Biochemistry, National Chung-Cheng University, 168 University Road, Min-Hsiung, Chiayi 621, Taiwan

[∥]Key Laboratory of Pesticide and Chemical Biology of Ministry of Education, College of Chemistry, Central China Normal University, Wuhan 430079, P.R. China

S *Supporting Information*

ABSTRACT: Nano contrast agents (Nano CA) are nanomaterials used to increase contrast in the medical magnetic resonance imaging (MRI). However, the related relaxation mechanism of the Nano CA is not clear yet and little significant breakthrough in relaxivity enhancement has been achieved. Herein, a new hydrophilic Gd-DOTA complex functionalized with different chain length of PEG was synthesized and incorporated into graphene quantum dots (GQD) to obtain paramagnetic graphene quantum dots (PGQD). We performed a variable-temperature and variable-field intensity NMR study in aqueous solution on the water exchange and rotational dynamics of three different chain lengths of PGQD. The optimal GQD with paramagnetic chain length shows a great improvement in performance on ^{1}H NMR relaxometric studies. *In vitro* results demonstrated that the relaxivity of the designed PGQD could be controlled by regulating the PEG length, and its relaxivity was ∼16 times higher than that of current commercial MRI contrast agents (e.g., Gd-DTPA), on a "per Gd" basis. The relaxivity of the Nano CA can be rationally tuned to obtain unmatched potentials in MR imaging, exemplified by preparation of the paramagnetic GQD with the enhanced T_1 relaxivity. The fabricated PGQDs with suitable PEG length got the best relaxivity at 1.5 T. After intravenous injection, its feeding process by solid tumor could even be monitored by clinically used 1.5 T MRI scanners. This research will also provide an excellent platform for the design and synthesis of highly effective MR contrast agents.

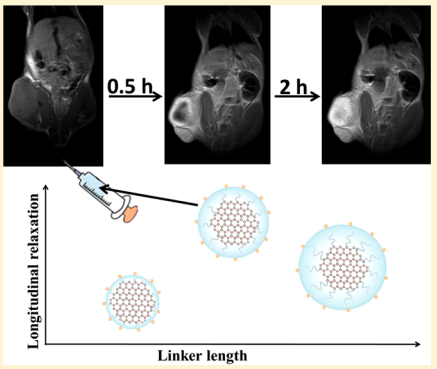

KEYWORDS: *Magnetic resonance imaging, graphene quantum dots, contrast agents, enhanced relaxivity*

Paramagnetic compounds are often used as contrast agents (CAs) in clinical MRI to enhance the contrast by selectively relaxing the water molecules near the compounds.[1] Among the different paramagnetic compounds used in contrast agents, Gd-DTPA is one of the most frequently used clinical agents because of its high thermodynamic and kinetic stabilities. However, the main defect of Gd-DTPA is its short circulation time, low relaxivity, and little specificity.[2,3] In that way, enhanced relaxivity of CAs with specific tissue detection are required to increase the efficiency of magnetic resonance imaging. Therefore, proteins,[4] liposomes,[5] dendrimers,[4] and nanoparticles[6−8] carrying high payloads of CAs have been developed to increase the MR signal. Gd-complex CAs were covalently incorporated to the structures of nanocarriers[9] to attain high relaxivity values and increase the circulation time. Among the various forms of multifunctional NP CAs, graphene quantum dots (GQD) have received considerable attention as a new type of nanoprobe due to the higher biocompatibility.[10] Owing to its luminescence stability, nanosecond lifetime, low toxicity, and high water solubility, GQD are attractive candidates for enhanced contrast bioimaging.[11−14]

An MRI is obtained by contrast between different biological tissues. T_1 MRI CAs reduce the longitudinal relaxation time, whereas T_2 MRI CAs shorten the transverse relaxation time. The efficiency of T_1 or T_2 MRI CAs is defined by r_1 or r_2 relaxivity, which is equal to the longitudinal $(1/T_1)$ and the transverse rate $(1/T_2)$. Relaxivity is simply increased in longitudinal relaxation rate after the introduction of paramagnetic compounds such as Gd-DTPA. It is normalized to the concentration of the paramagnetic metal ion (M), eq 1

$$r_1 = \frac{\Delta\left(\frac{1}{T_1}\right)}{[\mathrm{M}]} \quad (1)$$

Received: October 22, 2018
Revised: December 16, 2018
Published: December 18, 2018

DOI: 10.1021/acs.nanolett.8b04252
Nano Lett. 2019, 19, 441−448

Scheme 1. (a) Schematic of Gd Chelate with One Inner-Sphere Water Molecule Surrounded by Bulk Water[a]

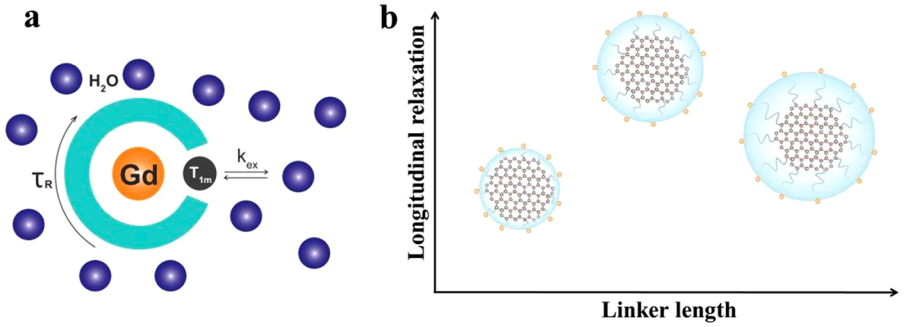

[a] τ_R refers to the rotational correlation time of the molecule, K_{ex} refers to the water/proton exchange rate and $T_{1,2e}$ refers to the relaxation times of the Gd electrospin. (b) The Gd rotation with the global motion of GQD may be influence by the linker PEG. The fabricated nanoparticles were named GQD-PEG_2-Gd, GQD-PEG_{12}-Gd, and GQD-PEG_{24}-Gd, which represented that the numbers of the repetitive unit, $-CH_2CH_2O-$, were 2, 12 and 24, respectively. By optimizing the rotation of Gd through controlling the different length of linker PEG, a MRI CA with the best longitudinal relaxation at 1.5 T was fabricated.

One of the major challenges in the field of Gd-based commercial MRI CAs is to improve the contrast for sensitive molecular imaging while minimizing the concentration of Gd^{3+}. Therefore, novel compounds which own strong proton relaxivity or provide better contrast for MR signal enhancement at lower doses are required. There are two ways to increase proton relaxivity: linking a number of gadolinium-chelate complexes together and rational design of the molecular structure that govern relaxivity. Relaxivity can be controlled by several factors, such as the paramagnetic properties of gadolinium, the external field, rotational diffusion, water exchange rate, inner and outer coordination sphere hydration, and the distance of paramagnetic ion to water proton. Combining eqs 2−4, for a small molecular CA, it is observed that the inner sphere contributions to the relaxivity can be significantly increased simply by prolonging τ_R (tumbling time),[15] where [M] is the concentration of Gd^{3+} ions in solution (in mM) and $1/T_{1,p}$ is the paramagnetic contribution to the relaxation rate, q represents the number of inner-sphere water molecules, T_{1m} and τ_m are the T_1 relaxation time and the residence time of inner sphere water molecules, respectively.

Theoretically, the T_1 relaxation can be improved by slowing the rotation rate of the MRI agent. As the $\omega_L^2\tau_{c1}^2$ term from eq 3 becomes more significant at high magnetic field, the effect of a slower rotation rate becomes more obvious, as shown in Scheme 1. The contrast enhancement of MRI CAs can be improved by slowing the motion of these contrast agents. The most frequently used strategies are the attachment of the small MRI CAs to macromolecules, such as protein, polymers, and nanoparticles, to slow the tumbling rate and thus increase the relaxivity, according to eqs 2−4 and Scheme 1. So we can optimize the rotation of Gd^{3+} through controlling the length of linker PEG

$$\frac{1}{T_{1,p}} = \frac{[M]q}{55.56T_{1m}} \quad (2)$$

$$\frac{1}{T_{1m}} = \frac{1}{T_1^{DD}} \propto \frac{3\tau_{c1}}{(1+\omega_L^2\tau_{c1}^2)} \quad (3)$$

$$\frac{1}{\tau_{c1}} = \frac{1}{\tau_m} + \frac{1}{\tau_R} \quad (4)$$

As a result of the slower rotation, the proton relaxivities of Gd-linked GQD are much higher than Gd smaller molecules. We performed a variable-temperature and variable-field intensity NMR study in aqueous solution on the water exchange and rotational dynamics of three different PEG chain lengths which linked paramagnetic Gd and GQD.

Superparamagnetic iron oxide nanoparticles (SPIO) have become the preferred nano CAs for T_2-weighted MRI.[16−21] Unfortunately, it is difficult to differentiate between SPIO-labeled area and other hypointense regions *in vivo*. To circumvent this problem, positive-contrast MRI pulse sequences, proposed for T_1-based contrast agents, inherently achieve "positive contrast" due to the nature of the imaging technique. A familiar example is gadolinium (Gd)-based complexes, which are known to generate hyperintense regions as a result of the enhanced longitudinal relaxation time (T_1) of nearby exchanging water protons.[22] In order to reduce the toxicity, Gd^{3+} ions are always chelated with multidentate ligands, such as DOTA (1,4,7,10-tetraazacyclododecane-1,4,7,10-tetraacetic acid) and DPTA (diethylenetriaminepentaacetic acid) molecules.[23] Large amounts of Gd^{3+} ion chelates are introduced during the clinical MRI procedure, because it has no targeting.

The installation of a targeting molecule to the multifunctional nanoparticulate CAs enhances their ability to recognize cancer cells. Series of targeting molecules were reported, such as peptides, antibodies, and aptamers.[24−27] Among these ligands, hyaluronic acid (HA) has been extensively used due to its biocompatible, biodegradable, and nontoxic behavior, and it can easily bind with high affinity to the hyaluronan (CD44) receptor which is overexpressed in nonsmall cell lung carcinoma (NSCLC).[28−30]

Here, we report the synthesis of a nanocomplex incorporating GQD, Gd^{3+}, and a typical anticancer drug doxorubicin (DOX) for magnetofluorescent imaging and theranostics. The designed composites not only significantly enhanced imaging contrast but have also been shown to function as a nanocarrier for intracellular drug delivery. First, DOTA was linked to fluorescent GQD via a bridge of diamino-terminated poly(ethylene glycol) (PEG diamine). After chelation with Gd^{3+} ions, the formed PGQD-HA composites (Scheme 1) generated MRI contrast on T_1-weighted scans. By optimizing the rotation of Gd^{3+} through controlling the length of linker PEG, an MRI CA with the best longitudinal relaxation at 1.5 T was fabricated

DOI: 10.1021/acs.nanolett.8b04252
Nano Lett. 2019, 19, 441−448

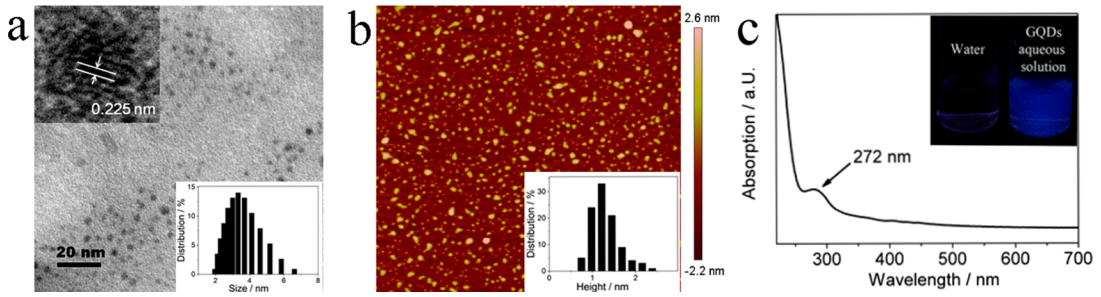

Figure 1. (a) TEM image and size distribution; inset of (a) is the HRTEM of GQD. (b) AFM image and height distribution of GQD. (c) UV−vis spectra of GQD (inset is a photograph of water and GQD aqueous solution under UV light with 365 nm excitation).

and the nanocomposites were named paramagnetic graphene quantum dots (PGQD). Second, to selectively target cancer cells, HA was further modified to the PGQD. The *in vivo* dynamic process of the nanoprobe was monitored at 1.5 T human MRI scanner. Results showed the fabricated PGQD-HA could selectively arrive at tumor fringe in 0.5 h and enter into tumor center in 2 h. Moreover, as a one-atom-thick graphitic carbon system, graphene-based materials are ideal for use as sheetlike vehicles to load anticancer drug DOX via π-conjugative interaction through the benzene ring. With the increased hydrophilicity and solubility of DOX in an acidic environment, drug release from PGQD-HA sheets can be observed in cancer cells. Accordingly, the resulting multifunctional nanoprobes not only offer good contrast enhancement for MRI and fluorescent imaging compared with small molecular-based CAs but, more importantly, enable an efficient mode of tumor-targeted theranostics.

Results and Discussion. As the most commonly used contrast agent for T_1-weighted MRI, the relaxivity and solubility of Gd^{3+} can be further optimized through conjugation to a biocompatible macromolecule such as a protein, polypeptide, dendrimer, and nanoparticle, which may increase the molecular tumbling time of Gd^{3+}due to the reduced number of degrees of freedom of large molecules in solution. In this study, paramagnetic Gd-DOTA was linked to GQD via a bridge of PEG.

First, water-soluble GQD were fabricated by the chemical oxidation and cutting of graphene oxide. Transmission electron microscopy (TEM) (Figure 1a) and atomic force microscopy (AFM) analysis (Figure 1b) revealed that the GQD exhibited a uniform size distribution with an average size of 3.35 nm. The high-resolution TEM (HRTEM) image (inset of Figure 1a) indicated the high crystallinity of the GQD with a lattice parameter of 0.225 nm, corresponding to (1120) lattice fringes of graphene. The edges of GQD seemed to be predominantly parallel to the zigzag orientation, which might dominant its strong luminescence. AFM image illustrated the topographic height of GQD was between 0.95 and 2.18 nm (Figure 1b), and more than 90% of the nanoparticles were less than 1.8 nm in height, indicating the synthesized GQD primarily consist of 1−3 layers. The UV−vis absorption spectrum of the resultant GQD showed an obvious absorption band at 272 nm[15] (Figure 1c). When exposed GQD was under an irradiation of 365 nm UV light, blue fluorescence was observed (Figure 1c, inset).

We propose that the Gd^{3+} rotation with the global motion of GQD may be influenced by the linker PEG. Thus, the relaxivity could be optimized by engineering an appropriate PEG. To achieve an efficient MRI contrast agent, the designed nanoparticles with three different lengths of PEG were studied. The fabricated nanoparticles were named GQD-PEG_2-Gd, GQD-PEG_{12}-Gd, and GQD-PEG_{24}-Gd, which represented that the numbers of the repetitive unit $-CH_2CH_2O-$ were 2, 12, and 24, respectively. As shown in Figure 2a, the longitudinal

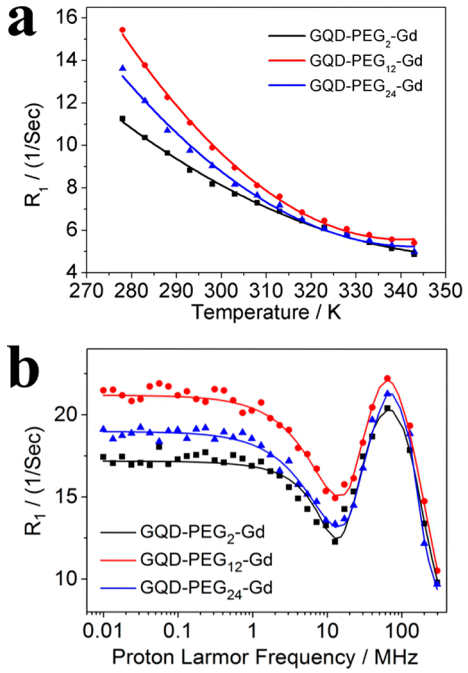

Figure 2. Characterizing the relaxometry of GQD-PEG_2-Gd, GQD-PEG_{12}-Gd, and GQD-PEG_{24}-Gd: (a) proton relaxivity at variable temperature and (b) ^{1}H NMRD profile at 25 °C.

relaxivity in all the three samples were decreased with the increasing temperature, this confirmed the hypothesis that the relaxivity of the fabricated nanoparticle are mainly controlled by molecular tumbling. The NMRD results showed the typical field peaks center were at 64 MHz (Figure 2b), indicating that the tumbling of the designed nanoparticles got the best matched resonance between proton and the magnetic field. It is worth mentioning that this is a remarkable difference from other Gd-based complexes which have the best relaxivity at 1−30 MHz;[30] the fabricated nanoparticles are better MRI contrast agents for commercially used 1.5 T (equal to 64 MHz) MRI scanner. Moreover, GQD-PEG_{12}-Gd yielded the highest longitudinal relaxivity among the three nanoparticles, demonstrating the highest contrast enhancement in MRI. Hence, GQD-PEG_{12}-Gd was chosen as the MRI contrast agent in the following experiments and was simplified as PGQD.

DOI: 10.1021/acs.nanolett.8b04252
Nano Lett. 2019, 19, 441−448

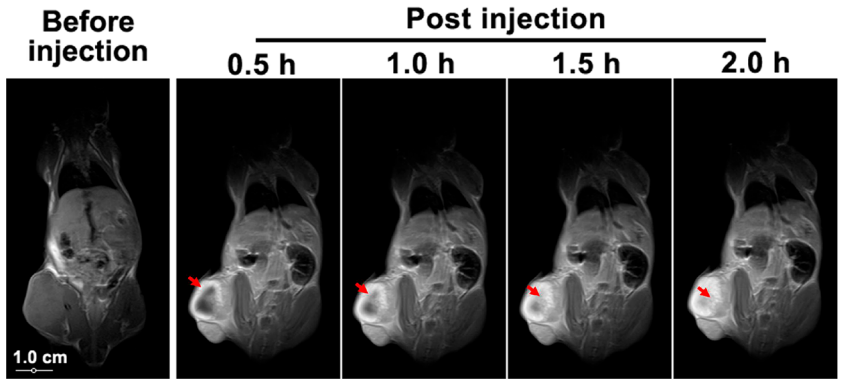

Figure 3. *In vivo* T_1-weighted magnetic resonance image of A549 tumor-bearing mice prior and postinjection of PGQD-HA by 1.5 T human MRI scanner. The tumor was lightened from fringe to center with the increasing postinjection time; this indicated the permeation process of the probe in tumor area.

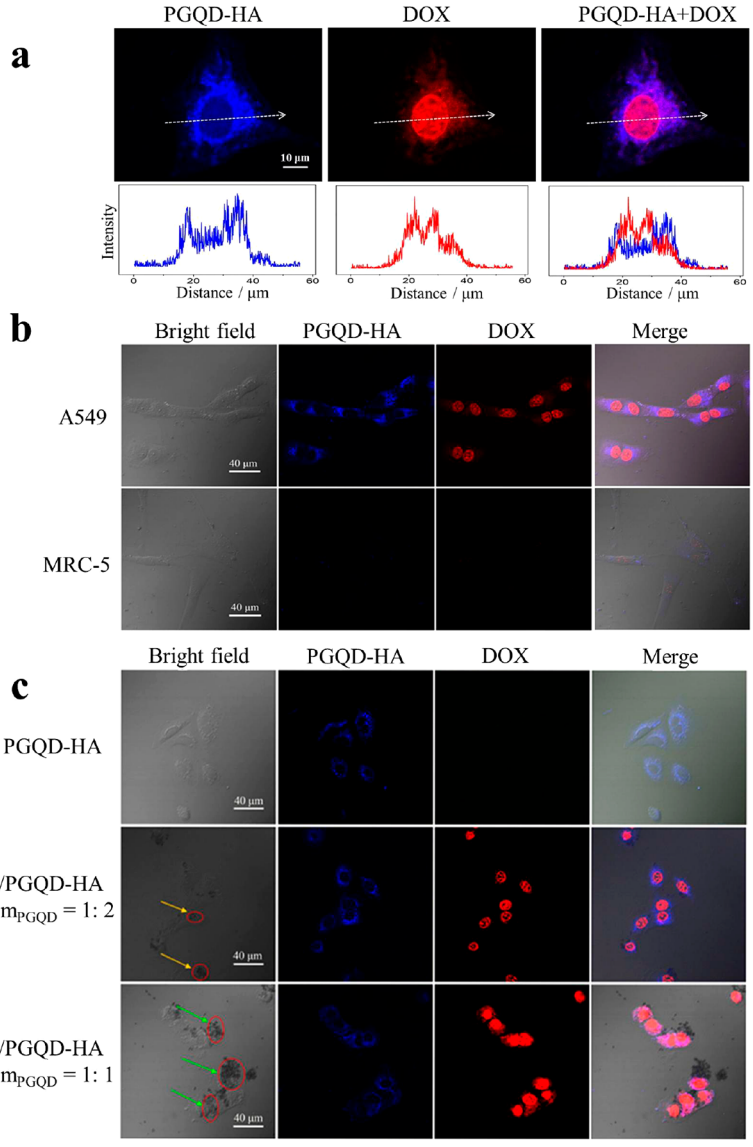

Figure 4. CLSM images evaluated the potential of DOX/PGQD-HA as an efficient anticancer agent: (a) the distribution of the vehicle PGQD-HA and anticancer drug DOX in A549 cells, (b) the selectivity of DOX/PGQD-HA between lung cancer cells A549 and embryonic lung cells MRC-5, and (c) the toxicity of PGQD-HA and DOX/PGQD-HA to A549 cells.

In order to increase the targeting ability, hyaluronic acid (HA) was further conjugated to the PGQD. To study the performance of the prepared PGQD-HA as MRI contrast agents, its relaxation property was assessed. After incubating

DOI: 10.1021/acs.nanolett.8b04252
Nano Lett. 2019, 19, 441−448

PGQD-HA with H_2O, human lung cancer cell (A549) and human embryonic lung cell (MRC-5), the measured protons T_1 were 200 ms, 800 ms and 1.8 s, respectively. According to T_1-weighted MRI results (Figure S8), the PGQD-HA enhanced a much stronger contrast of cancer cells than the normal MRC-5 cells at the same Gd^{3+} concentration, and this indicated selective uptake of PGQD-HA by A549 cells. The longitudinal relaxivities, achieved by determining the relaxation rate as a function of the concentration of Gd^{3+}, were found to be obviously increased for the PGQD-HA as compared to the clinical MRI CAs, such as Gd-DOTA. On the basis of the calculation of the concentration of Gd^{3+} ions, the relaxivity value (r_1) of the PGQD-HA was 16 times higher than the Gd-DOTA (Figure S6). The higher relaxivity of PGQD-HA is likely due to the increased molecular tumbling time of the Gd conjugated to GQD.

To evaluate the potentials of PGQD-HA for *in vivo* imaging, we have carried out MRI scans of mice intravenously injected with PGQD-HA. Because of the paramagnetic properties of Gd^{3+} ions, the conjugated PGQD-HA was expected to shorten the longitudinal relaxation time of protons and act as a T_1-weighted MRI contrast agent. The nude mice transplanted with A549 cancer cells were intravenously injected with PGQD-HA solution (5 μM of Gd^{3+} per kilogram of mouse body weight) via the tail vein 2 h prior to imaging (Figure S10), a very small (2.7 mm × 1.8 mm) lung tumor could be detected with high MRI contrast enhancement. The proton T_1 was notedly decreased from 1689 to 736 ms and the T_1-weighted images yield very good positive contrast. The image contrast was enhanced by the higher relaxation rate ($1/T_1$) in tumor tissue resulting from the accumulation of PGQD-HA. This illustrated the distinctive potential of PGQD-HA as a targeting contrast agent for T_1-weighted imaging, which is required for ultrasensitive imaging of cancer.

To be designed as a best CA for clinically used 1.5 T MRI, the MR property of PGQD-HA should be carefully estimated. A549 tumor bearing mice was anaesthetized and placed in 1.5 T MRI scanner and then intravenously injected with PGQD-HA solution (5 μM of Gd^{3+} per kilogram of mouse body weight) via tail vein. As shown in Figure 3, the tumor was totally indistinguishable with normal tissue in T_1-weighted MRI before PGQD-HA injection. After 0.5 h post injection, the tumor fringe was clearly traced. The bright field was gradually permeated to center until the tumor was entirely captured after 2 h injection. According to the enhanced permeability and retention (EPR) effect, the impaired lymphatic drainage, defective, and leaky vascular architecture and extensive angiogenesis greatly increased the permeability of micromolecular drugs and nanoparticles in solid tumor.[31,32] By tracing the PGQD-HA induced T_1-weighted MRI in 1.5 T MRI scanner, this phenomenon was real-time and dynamically monitored in A549 tumor bearing mice (Supporting Information Movie). Hence, the designed nanocomposite could selectively arrive at the targeted solid tumor, enter into the tumor center, as well as be monitored by commercially used 1.5 T MRI scanner. Furthermore, more types of tumors will be visualized in 1.5 T MRI by replacing targeting molecular HA.

In order to develop the probe with comprehensive application, more properties were explored. As a single layer two-dimensional structure with sp^2 hybridized carbon atoms, graphene-based materials have large and diffuse negatively charged electron clouds which can attract small aromatic molecules through $\pi-\pi$ stacking interactions. Because of its flexible and single atomic layer, both sides of GQD can load aromatic molecules. Herein, a commercial anticancer drug doxorubicin (DOX) was chosen to study the vehicular ability of the prepared PGQD-HA. Results from the fluorescence spectrum (Figure S11), electrochemical response (Figure S13), and UV adsorption (Figure S14) demonstrated the favorable DOX loading and pH-depended releasing capability of the PGQD-HA vehicle.

First, we analyzed the localization of vehicle and drug by CLSM images. After incubation with DOX/PGQD-HA for 10 h, blue fluorescence from PGQD-HA was clearly observed in the perinuclear region and cytoplasm of A549 cells, while red fluorescence from DOX accumulated in or around the nuclei (Figure 4a). When the DOX/PGQD-HA complex was endocytosed by cancer cells, the acidic surroundings would induce drug molecules (DOX) to be released from the carrier surface. Subsequently, the released DOX entered nucleus and reacted with nucleic acid, while the blue GQD stayed in the cytoplasm. As a result, the fluorescent intensity from PGQD-HA and DOX were totally different and complementary. Next, human embryonic lung cells (MRC-5) and human lung cancer cells (A549) were incubated in DOX/PGQD-HA culture medium at the same concentration for 4 h. The CLSM images (Figure 4b) revealed the good selectivity of DOX/PGQD-HA to A549 cells, which was consistent with MRI results (Figure S8). Negligible fluorescence has been observed from MRC-5 cells treated with DOX/PGQD-HA. Strong fluorescence from drug and vehicle indicated a large uptake of DOX/PGQD-HA by A549 cancer cells via receptor-mediated endocytosis. The therapeutic efficacy of DOX/PGQD-HA in the intracellular space was also assessed. As shown in Figure 4c, after A549 cells were treated with PGQD-HA for 10 h, blue fluorescence was clearly observed in the perinuclear region and cytoplasm of A549 cells, indicating that GQD could hardly penetrate into nuclei. When A549 cells were incubated with DOX/PGQD-HA (m_{DOX}/m_{PGODs} = 1:2) medium for 10 h, a red fluorescence appeared in the nucleus and perinuclear region. DOX was found scattered in both nuclear and cytoplasmic fluorescence measurements with an increased DOX/PGQD ratio. Meanwhile, we also observed that the membranes of A549 cells displayed signs of damage (Figure 4c, yellow arrows) after 10 h incubation with DOX/PGQD-HA, where some membranes of A549 cells even ruptured at a higher DOX concentration (Figure 4c, green arrows). These phenomena demonstrated that sequential delivery of DOX into A549 cells by DOX/PGQD-HA yielded a significant improvement of cancer cell killing efficacy. Information from MTT assay (Figure S16) also revealed the increased selectivity and high toxicity when the drug DOX loaded onto PGQD-HA vehicle.

In conclusion, the relaxivity of Gd chelates linked nanoparticles or macromolecule is always greater than Gd chelates itself. This phenomenon was well studied in nanoparticle-based MRI, however, its mechanism was paid little attention. In this work, Gd-DOTA was linked to GQD by a PEG bridge. The longitudinal relaxivity of the fabricated PGQD could be controlled through regulating the length of PEG. The ^1H NMR relaxometric studies revealed the tumbling of the designed nanoparticles got the best matched resonance between proton and the magnetic field at 1.5 T, and this demonstrated the PGQD would be an ideal contrast agent for the most widely used MRI scanner in clinical. A targeting molecular HA was further modified to the PGQD and injected into A549 tumor

DOI: 10.1021/acs.nanolett.8b04252
Nano Lett. 2019, 19, 441−448

bearing mice. The dynamic feeding process of PGQD-HA to solid tumor was well monitored by clinically used 1.5 T MRI scanner, including arriving at the fringe of solid tumor in 0.5 h, entering into the tumor gradually, and getting into tumor center in 2 h. Moreover, the drug loading and releasing ability of PGQDHA was also studied. In summary, a Gd-linked GQD was designed and fabricated for clinically used 1.5 T MRI scanner through relaxivity mechanism ratiocination, its functions, such as drug releasing, photothermal therapy, or photoacoustic imaging, could be further exploited.

Experimental Section. *Materials.* Graphene oxide was purchased from Nanjing XFNANO Materials Tech Co., Ltd. (Nanjing, China). *N*-(3-dimethylaminopropyl)-*N*-ethylcarbodiimide hydrochloride (EDC·HCl, 99%), *N*-hydroxysuccinimide (NHS, 97%), gadolinium(III) chloride hexahydrate ($GdCl_3 \cdot 6H_2O$, 99%), poly(ethylene glycol)bis(amine) (PEG-diamine, M_r 2000), and 3-[4,5-dimethylthialzol-2yl]-2,5-diphenyltetrazolium bromide (MTT, 98%) were purchased from Sigma-Aldrich (St. Louis, U.S.A.). Hyaluronic acid (HA, M_r 170−350 kDa) was purchased from Zirench Technology Co., Ltd. (Dalian, China). 1,4,7,10-Tetraazacyclododecane-*N*,*N*′,*N*″,*N*‴-tetraacetic acid (DOTA, 98%) was obtained from J&K Chemical (Beijing, China). All chemicals were used as received.

Instrumentation. The chemical composition of the GQD and PGQD-HA was determined using an ESCALAB 220i-XL X-ray photoelectron spectrometer (XPS) (VG Scientific Ltd.). The microstructure of the GQD was observed using transmission electron microscopy (TEM JEOL JSM-3010). Fourier transform infrared (FTIR) spectra are recorded on a Bruker tensor 37 spectrophotometer from 400 to 4000 cm^{-1}. AFM measurements were carried on Vecco digital instruments, di Innova. Samples for AFM measurements were prepared by spin coating MoS_2 and WS_2 solutions onto mica substrate. UV−vis absorption spectra were recorded in an Evolution 220 spectrophotometer (Thermo Fisher Scientific). Fluorescence spectra were recorded at room temperature on a Hitachi 7000 fluorescence spectrophotometer. Electrochemical measurements were performed on a PARSTAT 2273 advanced electrochemical system with a conventional three-electrode system comprising platinum wire as auxiliary electrode, saturated calomel electrode (SCE) as reference, and the modified glass carbon electrode (GCE) as the working electrode.

Cell Culture. Human lung adenocarcinoma cell line A549 and normal human lung fibroblast cell line MRC-5 were obtained from the Cell Bank of Shanghai Institute of Cell Biology, China. The A549 and MRC-5 cells were maintained in DMEM and MEM medium respectively, supplemented with 10% inactivated fetal bovine serum and 1% penicillin/streptomycin 10000 U/ml, and was grown in an incubator at 37 °C, supplied with 5% CO_2.

Cellular Uptake of PGQD-HA. Briefly, A549 cells were immersed in a medium with 50 $\mu g \cdot mL^{-1}$ of PGQD-HA for 3 h. Then, cells were centrifuged at 2000 rpm and washed with PBS one time. The cells were then fixed by a 2.5% solution of glutaraldehyde. Following washing with 1× PBS, the pellet was stained with osmium tetroxide. The pellet was then washed with 5× PBS. After a series of dehydration steps with ethanol (50%, 70%, 90%, and 100%), the pellet was cured in LR white resin (Electron Microscopy Sciences, Hatfield, PA) overnight at 70 °C. The resin-embedded pellet was then sectioned using a microtome and imaged by TEM.

Tumor Implantation. Adult female nude mice (average 20 g) were obtained from Hunan SJA Laboratory Animal Co., Ltd. All experiments conformed to animal care protocols and were approved by Animal Care and Use Committees at the Wuhan Institute of Physics and Mathematics, the Chinese Academy of Sciences. To induce a tumor, ∼2×10^6 A549 cells were suspended into 200 μL of PBS and injected into the lower back of lightly anesthetized mice (1% isoflurane/oxygen mixture).

^{1}H NMRD (Nuclear Magnetic Relaxation Dispersion) Profiles. ^{1}H NMRD profiles were measured on a SPINMASTER FFC-2000 (Stelar s.l.r.) fast-field-cycling NMR relaxometer covering magnetic fields from 2.34×10^{-4} to 0.94 T (corresponding to proton Larmor frequencies of 0.01−40 MHz) and required classical saturation-recovery experimental NMR techniques. All the samples contained 0.1 mmol/L Gd^{3+}; the concentrations of Gd^{3+} were determined by ICP-MS. The dead time of the spectrometer was ∼10 μs. The free induction decay was sampled with 1000 points after a 90° pulse with duration of 5.34 μs. The NMRD profiles were measured at 298 K.

Temperature Dependence of Proton Relaxivity. The temperature studies of T_1 relaxation were performed on a Bruker Nuclear Magnetic Resonance Spectrometer at the fixed field of 500 M Hz. The temperature was controlled by a BCU temperature control unit. In each case, 500 μL 0.1 mM aqueous solutions of GQD-PEG-Gd (calculated per gadolinium) was placed in 5 mm NMR tube, and the T_1 value was determined under 278−343 K. A modified Inversion recovery sequence given by (180°-G1-90-G2-G3-FID) was employed for the T_1 measurement.[33] To suppress the radiation damping, pulsed field gradients (PFG) were applied during the inversion time and before acquisition. G1 denotes the PFG applied during the whole inversion time with an amplitude of 33 mT/m, G2 and G3 denote the PFG applied before acquisition, which has the same amplitude of 33 mT/m but opposite sign; the duration of both G2 and G3 is 5 ms.

In Vivo MRI. Imaging experiments were carried out in a 1.5T human whole-body MRI Scanner (Avanto, Siemens Medical Solutions). The rf excitation was performed by a body coil, and signal detection was obtained with 4 cm diameter loop surface coil. Following induction of a mouse to the plane of anesthesia by chloral hydrate with intraperitoneal injection, the mouse was laid on the patient bed in the prone position. T_1-weighted MRI was achieved in the coronal plane by a multislice spin−echo sequence with the following parameters: FOV (field of view) = 100 × 100 mm, matrix = 384 × 288, slice thickness = 3 mm, TR/TE = 550/11 ms, averages = 4.

Fluorescence Microscopy. To measure the cellular uptake, A549 cells and MRC-5 cells were cultured in a 6-well chamber slide with one piece of cover glass at the bottom of each chamber. GQD, PGQD-HA, and DOX/PGQD-HA were introduced to the incubation solution at a GQD concentration at 50 $\mu g \cdot mL^{-1}$. To fix the cells, the glass was incubated in a 4% paraformaldehyde solution for 10 min. After that, the slides were washed with 1 × 3 distilled water, covered with antifluorescence quenching reagent, and visualized by a laser scanning confocal microscope Nikon A1 (Nikon, Tokyo, Japan).

Gd^{3+} Concentration (ICP-MS). Gd^{3+}concentrations of the PGQD were confirmed by inductively coupled plasma-mass spectrometry (ICP-MS, X Series 2, Thermo Fisher). After mixing with 1.5 mL concentrated nitric acid, the sample was

DOI: 10.1021/acs.nanolett.8b04252
Nano Lett. 2019, 19, 441−448

heated to 100 °C for 30 min. Then, the sample was diluted to 50 mL with distilled water. The standard solutions with the Gd^{3+} concentration of 1, 5, 10, 20, 50, 100, 200 ppm in 3% nitric acid were prepared, and a calibration curve was made by plotting the corresponding chromatographic peaks versus the Gd^{3+} concentrations. Stock solution of nanoprobe (0.1 mM) was diluted 100 times by 3% nitric acid. The Gd^{3+}concentration of the sample was obtained by applying the detected Gd^{3+} peak against the calibration curve.

■ ASSOCIATED CONTENT

Supporting Information

The Supporting Information is available free of charge on the ACS Publications website at DOI: 10.1021/acs.nanolett.8b04252.

Detailed synthetic protocols of graphene quantum dots and PGQD-HA, high-resolution XPS of GQD and PGQD-HA, FTIR spectra of the PGQD-HA, PGQD, and GQD, longitudinal relaxivity (r_1) of GQD-Gd-HA, photoluminescence spectra of GQD and PGQD-HA, ^{1}H NMRD profiles, temperature dependence of proton relaxivity, cellular uptake of PGQD-HA, *in vitro* and *in vivo* MRI, DOX loading and releasing, isotherms characterizing adsorption of DOX onto GQD, cell viability assay (PDF)

Movie of tracing the PGQD-HA induced T_1-weighted MRI in 1.5 T MRI scanner where this phenomenon was real-time and dynamically monitored in A549 tumor bearing mice (AVI)

■ AUTHOR INFORMATION

Corresponding Author

*E-mail: xinzhou@wipm.ac.cn. Phone:+86-027-87198802.

ORCID

Aidong Zhang: 0000-0002-7050-4648

Xin Zhou: 0000-0002-5580-7907

Author Contributions

Y.Y. and S.C. contributed equally to this work.

Notes

The authors declare no competing financial interest.

■ ACKNOWLEDGMENTS

This work was supported by the National Natural Science Foundation of China (81625011, 21575157, 21605158, 81227902), the National Key R&D Program of China (2017YFA0505400, 2016YFC1304704), K.C Wong Education Foundation and Key Research Program of Frontier Sciences, CAS (QYZDY-SSW-SLH018), Hubei Provincial Natural Science Foundation of China (2016CFB184, 2017CFA013). X.Z. thanks the National Program for Special Support of Eminent Professionals (National Program for Support of Top-notch Young Professionals)

■ REFERENCES

(1) Pierre, V. C.; Harris, S. M.; Pailloux, S. L. Comparing Strategies in the Design of Responsive Contrast Agents for Magnetic Resonance Imaging: A Case Study with Copper and Zinc. *Acc. Chem. Res.* **2018**, *51*, 342−351.

(2) Gulani, V. Gadolinium deposition in the brain: summary of evidence and recommendations. *Lancet Neurol.* **2017**, *16*, 564−570.

(3) Fraum, T. J.; Ludwig, D. R.; Bashir, M. R.; Fowler, K. J. Gadolinium-based contrast agents: A comprehensive risk assessment. *J. Magn. Reson Imaging* **2017**, *46*, 338−353.

(4) Villaraza, A. J. L.; Bumb, A.; Brechbiel, M. W. Macromolecules, Dendrimers, and Nanomaterials in Magnetic Resonance Imaging: The Interplay between Size, Function, and Pharmacokinetics. *Chem. Rev.* **2010**, *110*, 2921−2959.

(5) Lee, M. H.; Kim, E. J.; Lee, H.; Kim, H. M.; Chang, M. J.; Park, S. Y.; Hong, K. S.; Kim, J. S.; Sessler, J. L. Liposomal Texaphyrin Theranostics for Metastatic Liver Cancer. *J. Am. Chem. Soc.* **2016**, *138*, 16380−16387.

(6) Smith, B. R.; Gambhir, S. S. Nanomaterials for *In Vivo* Imaging. *Chem. Rev.* **2017**, *117*, 901−986.

(7) Chen, R.; Canales, A.; Anikeeva, P. Neural recording and modulation technologies. *Nat. Rev. Mater.* **2017**, *2*, 16093.

(8) Hu, Y.; Mignani, S.; Majoral, J. P.; Shen, M. W.; Shi, X. Y. Construction of iron oxide nanoparticle-based hybrid platforms for tumor imaging and therapy. *Chem. Soc. Rev.* **2018**, *47*, 1874−1900.

(9) Aime, S.; Castelli, D. D.; Crich, S. G.; Gianolio, E.; Terreno, E. Pushing the Sensitivity Envelope of Lanthanide-Based Magnetic Resonance Imaging (MRI) Contrast Agents for Molecular Imaging Applications. *Acc. Chem. Res.* **2009**, *42*, 822−831.

(10) Nurunnabi, M.; Khatun, Z.; Huh, K. M.; Park, S. Y.; Lee, D. Y.; Cho, K. J.; Lee, Y. K. In Vivo Biodistribution and Toxicology of Carboxylated Graphene Quantum Dots. *ACS Nano* **2013**, *7*, 6858−6867.

(11) Lin, J.; Chen, X. Y.; Huang, P. Graphene-based nanomaterials for bioimaging. *Adv. Drug Delivery Rev.* **2016**, *105*, 242−254.

(12) Shen, J. H.; Zhu, Y. H.; Yang, X. L.; Li, C. Z. Graphene quantum dots: emergent nanolights for bioimaging, sensors, catalysis and photovoltaic devices. *Chem. Commun.* **2012**, *48*, 3686−3699.

(13) Hu, S.; Chen, Y.; Hung, W.; Chen, I.; Chen, S. Quantum-Dot-Tagged Reduced Graphene Oxide Nanocomposites for Bright Fluorescence Bioimaging and Photothermal Therapy Monitored *In Situ*. *Adv. Mater.* **2012**, *24*, 1748−1754.

(14) Peng, J.; Gao, W.; Gupta, B.; Liu, Z.; Romero-Aburto, R.; Ge, L.; Song, L.; Alemany, L. B. M.; Zhan, X.; Gao, G.; Vithayathil, S. A.; Kaipparettu, B. A.; Marti, A. A.; Hayashi, T.; Zhu, J. J.; Ajayan, P. M. Graphene Quantum Dots Derived from Carbon Fibers. *Nano Lett.* **2012**, *12*, 844−849.

(15) Merbach, A; Helm, L; Toth, E. *The Chemistry of Contrast Agents in Medical Magnetic Resonance Imaging*, second ed.; Wiley, 2013.

(16) Ho, D.; Sun, X.; Sun, S. Monodisperse Magnetic Nanoparticles for Theranostic Applications. *Acc. Chem. Res.* **2011**, *44*, 875−882.

(17) N'Guyen, T. T. T.; Duong, H. T. T.; Basuki, J.; Montembault, V.; Pascual, S.; Guibert, C.; Fresnais, J.; Boyer, C.; Whittaker, M. R.; Davis, T. P.; Fontaine, L. Functional Iron Oxide Magnetic Nanoparticles with Hyperthermia-Induced Drug Release Ability by Using a Combination of Orthogonal Click Reactions. *Angew. Chem., Int. Ed.* **2013**, *52*, 14152−14156.

(18) Lee, J. H.; Jun, Y.; Yeon, S. I.; Shin, J. S.; Cheon, J. Dual-Mode Nanoparticle Probes for High-Performance Magnetic Resonance and Fluorescence Imaging of Neuroblastoma. *Angew. Chem., Int. Ed.* **2006**, *45*, 8160−8162.

(19) Gao, Z.; Hou, Y.; Zeng, J.; Chen, L.; Liu, C.; Yang, W.; Gao, M. Tumor Microenvironment-Triggered Aggregation of Antiphagocytosis 99mTc-Labeled Fe_3O_4 Nanoprobes for Enhanced Tumor Imaging *in Vivo*. *Adv. Mater.* **2017**, *29*, 1701095.

(20) Ma, T.; Hou, Y.; Zeng, J.; Liu, C.; Zhang, P.; Jing, L.; Shangguan, D.; Gao, M. Dual-Ratiometric Target-Triggered Fluorescent Probe for Simultaneous Quantitative Visualization of Tumor Microenvironment Protease Activity and pH *in Vivo*. *J. Am. Chem. Soc.* **2018**, *140*, 211−218.

(21) Zeng, J.; Jing, L.; Hou, Y.; Jiao, M.; Qiao, R.; Jia, Q.; Liu, C.; Fang, F.; Lei, H.; Gao, M. Anchoring Group Effects of Surface Ligands on Magnetic Properties of Fe_3O_4 Nanoparticles: Towards High Performance MRI Contrast Agents. *Adv. Mater.* **2014**, *26*, 2694−2698.

DOI: 10.1021/acs.nanolett.8b04252
Nano Lett. 2019, 19, 441−448

(22) Tóth, É.; Helm, L.; Merbach, A. *The Chemistry of Contrast Agents in Medical Magnetic Resonance Imaging: Relaxyvity of Gadolinium(III) Complexes: Theory and Mechanism*; Wiley: Chichester, 2012.
(23) Brücher, E.; Tircsó, G.; Baranyai, Z.;.Kovács, Z.; Shery, A. D. *The Chemistry of Contrast Agents in Medical Magnetic Resonance Imaging: Stability and Toxicity of Contrast Agents*; Wiley: Chichester, 2012.
(24) McNamara, J. O.; Andrechek, E. R.; Wang, Y.; Viles, K.; Rempel, R. E.; Gilboa, E.; Sullenger, B. A.; Giangrande, P. H. Cell Type-specific Delivery of siRNAs with Aptamer-siRNA Chimeras. *Nat. Biotechnol.* **2006**, *24*, 1005−1015.
(25) Lefkowitz, R. J. A Brief History of G-Protein Coupled Receptors. *Angew. Chem., Int. Ed.* **2013**, *52*, 6366−6378.
(26) Majumdar, S.; Siahaan, T. J. Peptide-mediated targeted drug delivery. *Med. Res. Rev.* **2012**, *32*, 637−658.
(27) Sudimack, J.; Lee, R. J. Targeted Drug Delivery via the Folate Receptor. *Adv. Drug Delivery Rev.* **2000**, *41*, 147−162.
(28) Weber, G. F.; Ashkar, S.; Glimcher, M. J.; Cantor, H. Receptor-ligand Interaction between CD44 and Osteopontin (Eta-1). *Science* **1996**, *271*, 509−512.
(29) Laurent, T. C.; Fraser, J. R. Hyaluronan. *FASEB J.* **1992**, *6*, 2397−2404.
(30) Toth, E.; et al. The Role of Water Exchange in Attaining Maximum Relaxivities for Dendrimeric MRI Contrast Agents. *Chem. - Eur. J.* **1996**, *2*, 1607−1615.
(31) Hanahan, D.; Folkman, J. Patterns and Emerging Mechanisms Review of the Angiogenic Switch during Tumorigenesis. *Cell* **1996**, *86*, 353−364.
(32) Overchuk, M.; Zheng, G. Overcoming Obstacles in the Tumor Microenvironment: Recent Advancements in Nanoparticle Delivery for Cancer Theranostics. *Biomaterials* **2018**, *156*, 217−237.
(33) Eykyn, T. R.; Payne, G. S.; Leach, M. O. Inversion recovery measurements in the presence of radiation damping and implications for evaluating contrast agents in magnetic resonance. *Phys. Med. Biol.* **2005**, *50*, N371−N376.

DOI: 10.1021/acs.nanolett.8b04252
Nano Lett. 2019, 19, 441−448